Exploring the potential of graphene oxide nanosheets for porous media decontamination from cationic dyes

Exploring the potential of graphene oxide nanosheets for porous media decontamination from cationic dyes

Ali Beryani[°], Carlo Bianco, Alessandro Casasso, Rajandrea Sethi, Tiziana Tosco[*]

DIATI – Politecnico di Torino, Corso Duca degli Abruzzi 24, 10129 Torino (Italy)

(*) corresponding author: tiziana.tosco@polito.it

(°) current address: Dept. of Civil, Environmental, and Natural Resources Engineering, Luleå Univ. of Technology, 97187, Luleå, Sweden. E-mail: ali.beryani@ltu.se

Published in:

Journal of Hazardous Materials

Accepted 6 October 2021

Available online 12 October 2021

DOI: 10.1016/j.jhazmat.2021.127468

Link:

https://www.sciencedirect.com/science/article/pii/S0304389421024365?pes=vor

Abstract

Graphene oxide (GO) nanosheets, often embedded in nano-composites, have been studied as promising materials for waste water purification, in particular to adsorb heavy metals and cationic organic contaminants. However, a broader range of potential applications of GO is still unexplored. This work investigated the potential applicability of GO for enhanced in-situ soil washing of secondary sources of groundwater contamination (i.e. the controlled recirculation of a washing GO suspension via injection/extraction wells). The laboratory study aimed at quantifying the capability of GO to effectively remove adsorb methylene blue (MB) from contaminated sand. The tests were conducted in simplified conditions (synthetic groundwater at NaCl concentration of 20 mM, silica sand) to better highlight the key mechanisms under study. The results indicated a maximum sorption capacity of 1.6 mgMB/mgGO in moderately alkaline conditions. Even though the adsorption of MB onto GO slightly reduced the GO mobility in the porous medium, a breakthrough higher than 95% was obtained for MB/GO mass ratios up to 0.5. This suggests that a very high recovery of the injected particles should be also expected in the field.

Keywords

methylene blue; adsorption; remediation; graphene oxide

1. Introduction

Graphene oxide (GO) nanosheets are an emerging carbon-based 2D nanomaterial composed by single- or multi-layer flakes, having nanoscale thickness and an extremely high specific surface area. GO nanosheets contain large amounts of oxygenated functional groups, including carbonyl, carboxyl, hydroxyl, and phenol on their edges and surfaces, and thus they can inherently develop a strong negative surface charge in a relatively broad range of hydrochemical conditions, and act as good sorbents for ionic and polar compounds in water solutions [1, 2]. Electrostatic interactions, π-π stacking and hydrogen bonds have been identified as the dominant adsorption mechanisms [3]. Such GO attributes have led to their application in many engineering and medical fields [4-6]. On the one hand, GO nanosheets act as excellent carriers for the delivery of various compounds through the human body for medical purposes [7-12]. On the other hand, GO are promising adsorbents for drinking water or wastewater treatment, to remove a wide range of environmental contaminants [13, 14], such as heavy metals (e.g. As^{3+}, Ni^{2+}, Cr^{6+}, Pb^{2+}, Cd^{2+}, Cu^{2+}, Zn^{2+}) [15-17], dye molecules (e.g. methylene blue, bromophenol blue, basic blue 41, basic red 18/46, and malachite green) [18-21], and pharmaceuticals (e.g. methadone, ibuprofen and other similar anti-inflammatory drugs) [22-24].

Disposal of dye-containing wastewater produced by various industries (e.g. textile, paper, printing, cosmetics, food, pharmaceuticals, etc.) may pose serious health and environmental concerns if discharges are not under control [25]. Several studies showed that dye-contaminated water can be effectively treated via adsorption onto natural and synthetic sorbents, e.g. fly ashes [26, 27], calcine diatomite [28] and numerous carbon-based sorbents, including activated charcoal [29], carbon monoliths and nanocrystalline cellulose [30], activated carbon, carbon nanotubes, and graphene oxide [31].

At the moment, GO nanosheets have been proposed predominantly for the batch treatment of dye-contaminated wastewater as a lone material [19, 32, 33], incorporated in GO-based sponge materials [34, 35] or in magnetic [36-38] and non-magnetic [39] nanocomposites. Fewer applications envisioned the incorporation of GO in adsorbent porous beds [40, 41] or membranes [42] for in-line water treatment. These water purification technologies could benefit from the GO high sorption capacity toward a broad range of environmentally relevant substances. Among the possible options, in situ groundwater remediation is a prominent one. In this work we propose the application of GO for in situ treatment of contaminated aquifer systems, and present the laboratory-scale studies necessary as a first step toward the development of this technology.

GO nanosheets can be stably suspended in water, even at relatively high concentrations, and possess a considerable mobility in porous media [6, 43-47]. Moreover, their colloidal stability and mobility in the porous medium are significantly affected by the hydrochemical parameters (e.g. ionic strength and pH) and by the flow velocity [48-51]. All these characteristics suggest that GO nanosheets represent a promising nanomaterial for a controlled injection and delivery in the subsoil. In particular, the GO high sorption capacity toward a broad range of hydrophilic compounds indicates that this material has a good potential for being employed in a novel GO-assisted soil flushing, where GO suspensions are continuously recirculated in the subsoil using transects of injection and extraction wells. To unlock the potential of GO nanosheets for this application, the first key steps include (i) verify and quantify the capability of GO nanosheets to adsorb the target contaminant; (ii) study the mobility of the contaminant-loaded GO nanosheets in the porous media; (iii) evaluate the capability of GO to accelerate the desorption of the target contaminant from the contaminated soil.

This work follows these preliminary steps at the laboratory scale. Methylene blue (MB) was here selected as a model cationic pollutant, representative of a broad range of contaminants

of concern. MB is a common aromatic, water-soluble cationic dye, which has been reported as a relevant pollutant of water resources, with adverse effects on humans and on the aquatic organisms, such as increasing heartbeat, diarrhea, vomiting, shock, cyanosis, quadriplegia, jaundice, and tissue necrosis in human body [52]. MB is mainly used in the textile industry for cotton, silk and wool coloring, and in the paper industry for paper printing [53]. The capability of GO to adsorb MB has been already reported in the literature [18, 33, 54, 55]. Conversely, to date very few studies have addressed the co-transport of GO and adsorbing solutes in porous media. The recent literature on the co-transport of GO and heavy metals showed that the mobility of Pb^{2+} and Cd^{2+} [56, 57], U^{6+} [58], Cu^{2+} [59] and As^{3+} [60] can be significantly enhanced by GO nanosheets, which act as carriers and can also help remobilizing the heavy metals when already adsorbed on the porous medium. Co-transport with bacteria and clays were also reported [61, 62]. However, to our best knowledge, no study is available concerning the co-transport of GO and organic (hydrophilic) compounds, such as MB, in saturated porous media, nor on the use of GO to desorb organic compounds from soil matrices. This study contributes to fill these knowledge gaps with laboratory tests including (i) batch tests, aimed at assessing the capability of GO to adsorb MB, and identifying the optimal operating conditions that maximize adsorption without hindering GO colloidal stability; (ii) column co-transport tests, aimed at determining the key parameters controlling the co-transport and retention of MB-loaded GO nanosheets in saturated porous media, (iii) column removal tests, aimed at evaluating the efficacy of GO as a washing agent to remediate MB-contaminated sand columns.

2. Materials and Methods

2.1. Materials

High purity methylene blue (MB) was purchased in powder form from Alfa Aesar (Karlsruhe, Germany). Single layer GO nanosheets (nominal composition: 49-56% w/w C, 41-50% O, 0-1% H, and 2-4% S; nominal lateral size of 15.4±1.1 μm; nominal thickness of 0.8-1.2 nm) were provided by Graphenea Inc. (Spain) in the form of a concentrated aqueous suspension at 4 mg/mL. The specific surface area of this GO was previously measured via BET analysis and was found equal to 14±1.6 m^2/g [63].

Quartz sand (Sibelco, Italy) with grain size in the range 0.3~1.0 mm (d_{10}= 0.4 mm, d_{50}=0.75 mm) was used in column transport tests. To remove possible impurities (organic residual, oxides and hydroxides), the sand was thoroughly cleaned prior use following these steps: cyclic ultra-sonication and rinsing with tap water, one-day soaking in 10% (v:v) nitric acid solution, cyclic ultra-sonication and rinsing in tap water, cyclic ultrasonication and rinsing with deionized water, degassing in a vacuum chamber to release residual air micro bubbles.

MB and GO concentrations were measured using UV–visible spectroscopy analysis (Specord S600, Analytik Jena, Germany) with different procedures depending on the test, as detailed in the next sections. The GO zeta potential (ζ) was measured using Dynamic Light Scattering (Zetasizer Nano ZSP, Malvern Instruments, UK). The sand zeta potential was measured following the method presented by [64].

2.2. Preparation of MB-loaded GO suspensions

NaCl concentration of 20 mM and pH of 8.5 – 9 (adjusted using NaOH) were adopted for all suspensions (unless otherwise stated) based on previous studies [31, 47], which suggest a good GO colloidal stability at alkaline pH (8.5- 9) for NaCl solutions up to 30 mM.

All suspensions of MB-loaded GO nanosheets were prepared as follows. An aliquot of the GO stock suspension (4 mg/mL) was diluted in NaCl 20 mM solution to the desired GO concentration (C_{GO} in the range 9 to 80 mg/L, depending on the test). NaOH was then dosed to reach a pH of 8.5. The GO lateral size was adjusted to 1~1.2 μm via probe sonication (UP200S, Hielscher Ultrasonics GmbH, Germany), following the approach described in Beryani et al. [47]. Then, MB was added to reach the desired concentration (10 to 97 mg/L, depending on the test). The suspension was stirred for 30 minutes on a magnetic stirrer. According to preliminary kinetic pre-tests (not reported), and coherently with the literature [55], MB adsorption was observed to be a fast process, and in all tested conditions equilibrium between phases was reached in 5 mins, or less.

2.3. MB batch adsorption tests on GO nanosheets

Batch tests were carried out to evaluate the capability of GO to adsorb MB dissolved in water, to study the colloidal stability of MB-GO suspensions and to develop a reliable method to estimate the concentration of GO nanosheets, adsorbed MB and free (dissolved) MB from UV-vis data. Batch adsorption tests were performed varying MB and GO concentration. For fixed GO concentration (9, 20, 30, 50 or 80 mg/L), different doses of MB (up to a MB/GO mass ratio above 1) were added to the GO suspension. Immediately after the sample preparation, different aliquots of the suspension were collected for the following analyses: (i) without further treatment, for DLS and UV-vis spectrophotometry (to determine the GO and adsorbed MB concentrations, respectively C_{GO} and $C_{MB,ads}$); (ii) after filtration with 0.2 μm PTFE filters, again DLS (to exclude the presence of residual GO nanosheets in filtered samples) and then UV-vis spectrophotometry (to determine the free MB concentration, $C_{MB,free}$).

On selected samples, the colloidal stability of MB-loaded GO nanosheets was also monitored over time using DLS: after mixing on the stirrer, an aliquot of the MB-loaded GO sample was transferred in the DLS cuvette and the Z-average (assumed representative of the average particle size) was monitored over time for two hours to identify potential formation and growth of aggregates. Although the Z-average does not coincide with the real size of GO nanosheets [65], due to the non-spherical shape of thew GO nanosheets, this metric, read in terms of size trend in time, is useful to assess whether particles aggregate or not. Fourier transform infrared (FT-IR) transmission spectra (Bruker FTIR Equinox 55 spectrometer, equipped with a MCT cryo-detector, Germany) were measured for clean GO and MB-loaded GO to elucidate the MB-GO interaction mechanisms.

2.4. Column tests: co-transport of MB-loaded GO

A Plexiglas cylinder (L=10 cm, D=1.6 cm) was wet-packed with clean silica sand following the protocol reported by [66]. Columns were run vertically with bottom-to-top flow. The column tests were performed at a constant flow rate of 1.63×10^{-8} m^3/s (Darcy's velocity 8.1×10^{-5} m/s) following this protocol:

1) Pre-equilibration with deionized water (DIw) for at least 7 pore volumes (PVs);
2) Pre-injection with background electrolyte solution (20 mM NaCl) for 8 PVs;
3) Injection of the MB-loaded GO suspension in background electrolyte solution (20 mM NaCl) for 7.5 PVs;
4) Flushing with a particle-free 20 mM NaCl solution for 4 PVs.

The injected concentrations of MB and GO (respectively, $C_{0,MB}$ and $C_{0,GO}$) were selected based on the results of the batch adsorption tests. Before being injected, all

suspensions/solutions were degassed in a vacuum chamber to remove residual dissolved air. During the experiments, the full UV-vis spectra of the column inflow and outflow were continuously measured with a frequency of 30 seconds using the UV-Vis spectrophotometer equipped with flow-through quartz cells with 5 mm light path (Hellma, Germany). The NaCl breakthrough curve measured before injection at a wavelength of 198.5 nm (step 2 of the column test protocol) was least-squares fitted with the classical advection-dispersion equation for unreactive solutes using the software MNMs [46, 67]. The effective porosity and dispersivity of the sand-packed columns were respectively estimated equal to 0.49±0.02 and $5.16(\pm 0.8)\times 10^{-4}$ m.

2.5. Column tests: MB removal from loaded sand via GO injection

A second set of column tests was performed to investigate the GO capability to remove MB pre-adsorbed on sand grains. The experimental protocol for these tests included the following steps:

1) Pre-equilibration with deionized water (DIw) for at least 7 pore volumes (PVs) (not reported in the graphs);
2) Pre-injection with background electrolyte solution (20 mM NaCl) for 8 PVs (not reported in the graphs);
3) Injection of MB solution ($C_{0,MB}$ = 25 mg/L, 20 mM NaCl) for 26 PVs;
4) Flushing #1 with background electrolyte solution (20 mM NaCl) for 6 PVs, to promote elution of free MB molecules in the liquid phase and initiate desorption;
5) Flushing #2 with washing suspension/solution for 14 PVs. Depending on the tests, the washing solution was GO-free DIw, GO dispersed in DIw, or GO dispersed in NaCl 20mM. When present, GO was injected at a concentration of 50 mg/L.

The GO suspensions employed in these column tests were prepared following the protocol described in section 2.2 (excluding the MB loading). The column packing procedure, discharge rate and inflow/outflow monitoring were the same as described in section 2.4.

3. Results and Discussions

3.1. GO - MB interactions and their effects on FT-IR and UV-vis spectra

The analysis of the absorbance spectra of GO, MB and MB-loaded GO obtained from FT-IR and UV-Vis spectroscopy provided insight into the interactions between GO and adsorbed MB (Figure 1).

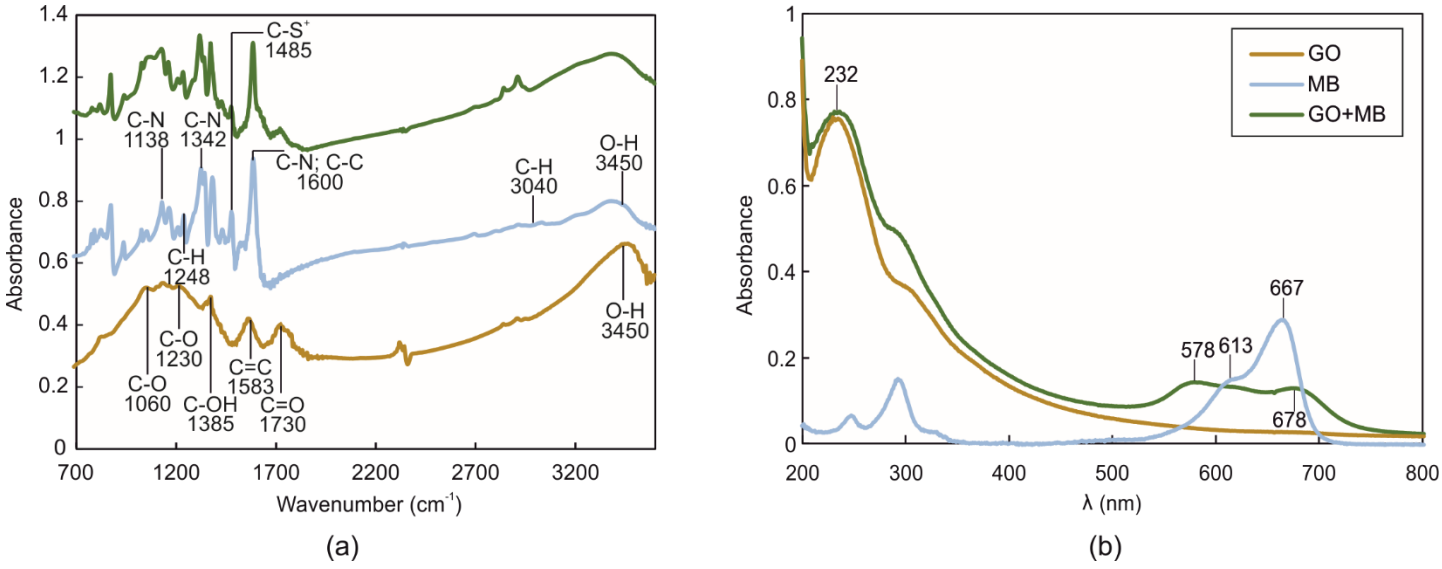

Figure 1: Characterization of bare GO (brown), MB (blue), and MB-loaded GO (green) in water: (a) FT-IR and (b) UV-Vis spectra. In all suspensions/solutions the concentrations were C_{GO} = 20 mg/L and C_{MB} = 5 mg/L.

FT-IR transmission spectra of bare GO confirmed the existence of different functional groups (i.e. epoxide, carbonyl, carboxyl and hydroxyl) on the surface of the GO nanosheets (Figure 1a). Comparing the FT-IR spectra of MB alone and MB-loaded GO, it appears that the intensity of $C=S^+$ stretching bond of MB central heterocycle (at wavenumbers 1356 and 1495

cm^{-1}) and the intensity of C=O stretching bond of carboxyl and carbonyl groups of GO (at 1730 cm^{-1}) both decline after MB adsorption. This observation can be associated with the electrostatic interaction between positively charged sulfur moiety of MB molecules and negatively charged -COOH functional groups of GO [32, 68, 69]. Moreover, the π–π interaction between the C=C stretching in MB and GO aromatic rings may partake in the adsorption process [9, 68, 70, 71]. Also the slight reduction of C=C stretching bond intensity in GO-MB spectrum at around 1600 cm^{-1} compared to MB spectrum may be attributed to the π–π interaction.

The UV–vis absorbance spectrum of the bare GO aqueous dispersion (Figure 1b) showed a main peak at λ=232 nm and a shoulder peak at around λ=295 nm, which can be respectively attributed to π-π^* transition of C=C bonds, and n-π^* transition of C=O bonds. In the presence of MB adsorbed on the GO nanosheets, new secondary peaks at 578 and 678 nm appeared, which were not present in the spectra of MB aqueous solutions (which conversely showed peaks at 613 nm and 667 nm). These peaks can be associated to the chemical bonds between MB and GO [70]. In particular, the peak at 678 nm is attributed to the overlap of π-clouds of GO and MB [72]. Its intensity increased with increasing concentration of adsorbed MB for low to moderate MB loading, whereas high MB concentrations lead to saturation of the band intensity. Conversely, the 578 nm peak can be attributed to the close packing between MB in the upper and lower faces of the GO sheets [72]. For bare GO, the absorbance was linear with GO concentration in the entire range of explored wavelengths (calibration curves reported in Supporting Information). Since for freely dissolved MB a negligible absorbance was measured in the region 380-440 nm, the measurements at λ=420 nm were selected for the calculation of GO concentration.

3.2. Batch adsorption tests

Batch tests at different GO concentration and MB/GO initial dose were performed to assess the capability of GO nanosheets to adsorb MB, to study their colloidal stability, and to identify the best operating conditions for column tests. In the tested conditions (i.e. NaCl 20 mM, pH≈8.5), GO nanosheets were stably dispersed in water in the absence of MB, with Zeta potential (ζ) equal to -50±4 mV. Conversely, when MB was added to the suspensions, the MB/GO dose played an important role also in the colloidal stability: the Zeta potential increased with increasing the MB concentration, reaching positive values for MB/GO ratio higher than 1, due to the progressive saturation of the GO surface by the MB cations. An example of the Zeta potential trend with increasing MB concentration is reported in Supporting Information (Figure S1).

3.2.1. MB adsorption and impact on colloidal stability

The capability of GO to adsorb MB was assessed using UV-vis spectrometry. Selected UV-vis spectra for C_{GO} = 50 mg/L and 9 mg/L at varying MB/GO mass ratio are reported in Figure 2.

In the tests performed with C_{GO} = 50 mg/L (Figure 2a), for MB/GO < 0.5 (green curves) the spectra rose with increasing MB concentration, with a shape analogous to that of the MB-loaded GO spectrum reported in Figure 1b. The peak at 578 nm (characteristic of adsorbed MB) increased with increasing C_{MB} (Figure 2c), whereas no evident peak at 667 nm (characteristic of free MB) was observed. These qualitative observations suggest that the suspension was colloidally stable for MB/GO<0.5, with negligible free MB. The absence of detectable dissolved MB was confirmed by UV-vis measurements on filtered samples, free of MB-loaded GO nanosheets (Figure 3a). The absence of significant aggregation was confirmed

by time-resolved DLS measurements, that showed no significant trend in size over 2 hours for samples with MB/GO < 0.5, and by visual inspection of the samples (see examples on selected batch tests reported in Supporting information, in Figures S3 and S4 and Table S1).

For a better insight, Figure 2c reports the trend of the absorbance at 420 nm and 578 nm as a function of MB concentration: the absorbance at 420 nm (predominantly due to GO nanosheets) remains almost constant for MB/GO<0.5, further confirming that GO nanosheets are stably dispersed in solution in this MB/GO range. Conversely, the absorbance at 578 nm (due to both GO nanosheets and adsorbed GO) increases linearly with MB concentration, and is due to two contributions: a constant value due to the constant concentration of GO nanosheets, and a second linear component increasing with increasing absorbed MB concentration (compare also the black curve corresponding to bare GO and the green curves of MB-loaded GO in Figure 2a).

The trends changed as the MB/GO ratio was increased above 0.5. The spectra declined in intensity (see orange/yellow curves in Figure 2a), even though no evident peak at 667 nm was observed in the spectra even in this case. This behavior suggests that partial aggregation and sedimentation occurred for MB/GO > 0.5, but MB was still predominantly adsorbed on GO nanosheets, without significant free MB in solution. The absence of free MB in solution was confirmed by the measurements on filtered samples (Figure 3a).

Further increasing the MB/GO ratio above 1 resulted in a fast and almost complete sedimentation of the GO nanosheets, and thus the spectra were measured only on filtered samples, which confirmed the presence of free MB for MB/GO > 1 (Figure 3a).

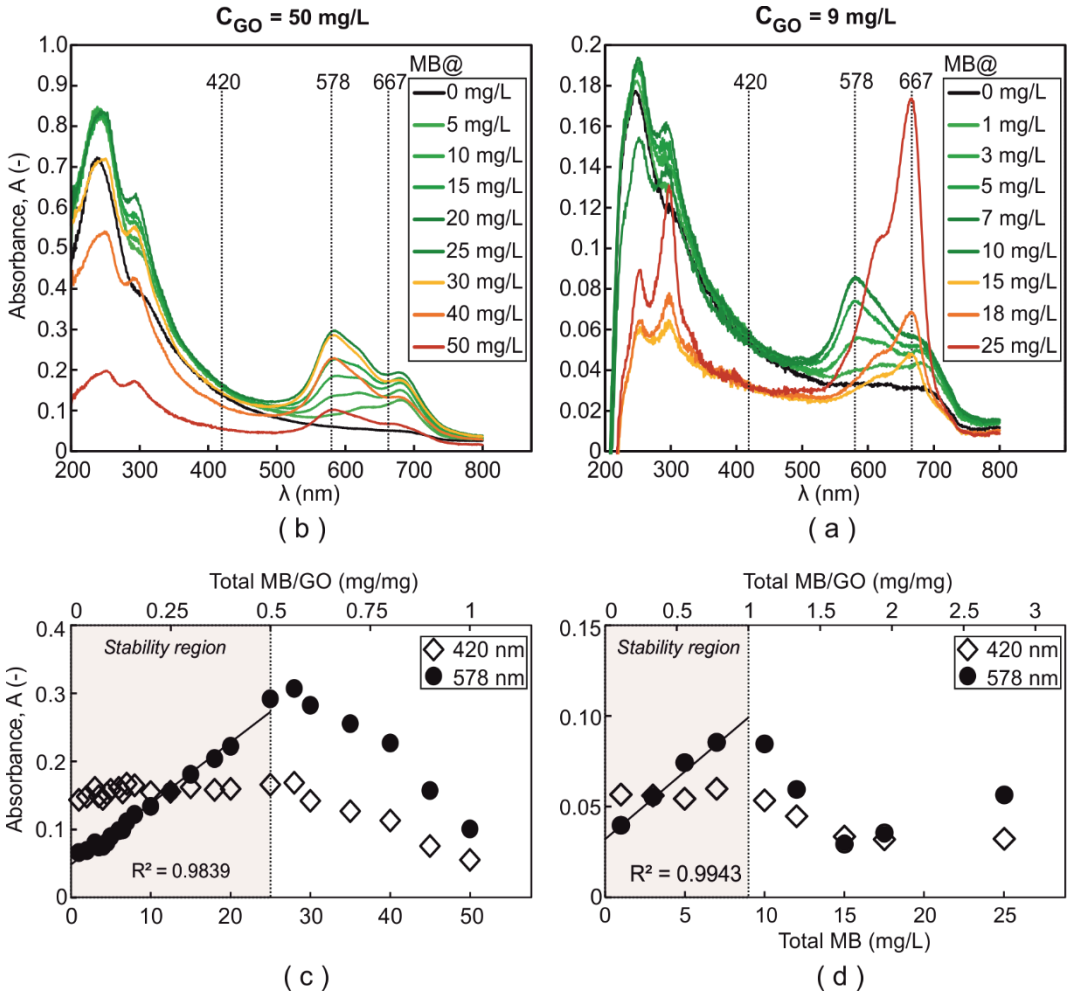

Figure 2: Adsorption batch tests. (a-b): UV-vis spectra for (a) C_{GO} = 50 mg/L and (b) C_{GO} = 9 mg/L with varying the total (initially dosed) MB concentration, C_{MB}. Green spectra correspond to colloidally stable suspensions, orange/red spectra to unstable samples. (c-d): trends of peak absorbance at λ = 420 nm (empty diamonds) and λ = 558 nm (black circles) reported as a function of the total C_{MB} (bottom axes) and MB/GO ratio (top axis), again for suspensions prepared with (c) C_{GO} = 50 mg/L and (d) C_{GO} = 9 mg/L. The grey areas identify the regions where the suspensions are colloidally stable, the black lines fit linearly the trend of the absorbance at 578 nm in the stability region.

To confirm and extend the results obtained for C_{GO} = 50 mg/L, the batch adsorption tests were performed also at C_{GO} = 9, 20, 30 and 80 mg/L. The results for C_{GO} = 9 mg/L are reported in Figure 2b and d. In this case the tests could be extended up to MB/GO = 2.7 with GO partly remaining in suspension, thus allowing the measurement of full spectra also in the range MB/GO >1. The data for C_{GO} = 9 mg/L showed trends similar to those discussed for C_{GO} = 50 mg/L: also in this case a stability region exists where GO nanosheets were stably dispersed (compare the initial constant trend of the absorbance at 420 nm in Figure 2d), the spectra rose

with MB concentration (see green curves in Figure 2b), the peak at 578 nm linearly increased with MB concentration, and no evident peak at 667 nm was registered, suggesting a negligible presence of free MB. However, for C_{GO} = 9 mg/L this stability region extended up to MB/GO approximately equal to 1. Above this ratio (orange/red curves in Figure 2b), a decline in the spectra was observed, suggesting a partial sedimentation of the suspensions, confirmed by the decline of the absorbance at 420 nm (Figure 2d). At the same time, the peak at 667 nm rose. The absorbance at 578 nm (Figure 2d) was linear with the MB concentration for MB/GO < 1 (stability region). As MB/GO rose above 1, the absorbance at 578 nm first declined due to GO sedimentation, and then showed a new rise due to the presence of free MB. This behavior is consistent with the non-negligible absorbance of MB solutions at 578 nm showed in Figure 1b. Consequently, for MB/GO >1 the absorbance at 578 nm is given by three contributions: GO nanosheets, absorbed MB and freely dissolved MB.

The tests performed at C_{GO} = 20, 30 and 80 mg/L (full spectra not reported, see Figure S5 in Supporting Information for peak absorbance trends) all confirmed the existence of a colloidal stability region, which extended up to approximately MB/GO = 1 for low GO concentrations (C_{GO} up to 20 mg/L) and approached MB/GO = 0.5 for higher C_{GO} values. Conversely, in all conditions a non-negligible concentration of freely dissolved MB was observed only above MB/GO = 1, regardless the GO concentration.

3.2.2. Adsorption isotherm

Based on the qualitative observations discussed in the previous section, a quantitative estimation of MB adsorption on the GO nanosheets can be obtained combining information from multiple UV-vis wavelengths. To this aim, the absorbance at λ = 420 nm and λ = 578 nm were used (absorbance unprocessed data are reported in Supporting Information in Figure

S5). As discussed above, the absorbance at 420 nm (A_{420}) shows a linear trend with C_{GO} as it is predominantly due to the GO nanosheets. For colloidally stable suspensions, the absorbance at 578 nm (A_{578}) is given by the sum of the absorbance due to GO nanosheets ($A_{578,GO}$) and a second component ($A_{578,dep} = A_{578} - A_{578,GO}$) which increases linearly with increasing the concentration of adsorbed MB ($C_{MB,ads}$). It is reasonable to assume that, even for colloidally unstable samples (i.e. outside the stability region), the two contributions to A_{578} due to GO nanosheets and adsorbed MB still remain linear with the respective concentrations, if no free MB is present. Conversely, in the presence of free MB the picture is further complicated and the relationships are not linear anymore.

Given the described UV-vis spectrum characteristics for MB-loaded GO, it is possible to identify the conditions to discriminate the presence/absence of freely dissolved MB, and to write the equations to calculate the concentration of adsorbed MB.

In the absence of freely dissolved MB, the ratio $A_{578,dep}/A_{420}$ is expected to be linear with the total (dosed) MB/GO ratio, and to deviate from linearity when free MB is present in the water phase (i.e., for MB/GO > 1), due to the change in the shape of the spectrum (Section 3.1). This assumption is confirmed by the ratios $A_{578,dep}/A_{420}$ calculated for all tests (see examples in Supporting information in Figure S6).

As a consequence, batch sorption UV-vis spectra were processed as follows:

- In the range where $A_{578,dep}/A_{420}$ was linear with the MB/GO ratio (i.e. when the presence of freely dissolved MB was negligible), the volume concentration of adsorbed MB, $C_{MB,ads}$ (mass of adsorbed MB in suspension per unit volume of sample), and suspended GO nanosheets, C_{GO} (mass of suspended GO per unit volume of sample), were calculated solving this system of equations:

$$\begin{cases} A_{420} = \alpha_{420,GO} \cdot C_{GO} + \alpha_{420,MBads} \cdot C_{MB,ads} \\ A_{578} = \alpha_{578,GO} \cdot C_{GO} + \alpha_{578,MBads} \cdot C_{MB,ads} \end{cases} \quad \text{(eq. 1)}$$

where $\alpha_{578,MBads} \cdot C_{MB,ads}$ corresponds to $A_{578,dep}$ defined above. The α_i proportionality coefficients were determined as follows:

- $\alpha_{420,GO}$ and $\alpha_{578,GO}$ were obtained via least-squares fitting of A_{420} vs C_{GO} and A_{578} vs C_{GO}, respectively, for all samples with $C_{MB} = 0$ (see calibration curves in Supporting Information in Figure S2);
- $\alpha_{420,MBads}$ and $\alpha_{578,MBads}$ were obtained via least-squares fitting of $A_{420,dep}$ vs $C_{MB,ads}$ and $A_{578,dep}$ vs $C_{MB,ads}$, respectively, for all samples in the stability region, i.e. MB/GO < 1 for C_{GO} = 9 and 20 g/L, and MB/GO < 0.5 for C_{GO} = 30, 50, 80 g/L.

The mass concentration of adsorbed MB (S_{MB}, mass of adsorbed MB per unit mass of GO) was then calculated as $C_{MB,ads}/C_{GO}$, to get rid of the effect of GO sedimentation.

- In the range where $A_{578,dep}/A_{420}$ was not linear with the MB/GO ratio, the concentration of free MB in solution ($C_{MB,free}$) was measured on filtered samples, and the mass concentration of adsorbed MB (S_{MB}) was calculated with a mass balance from this measurement.

Figure 3b shows the results of MB adsorption experiments on GO nanosheets (C_{GO} = 50 mg/L) in terms of S_{MB} as a function of the total (dosed) MB/GO ratio, calculated as described above. The results of Figure 3b confirm that GO nanosheets were highly effective in adsorbing MB under the tested conditions. For total MB/GO < 1, the MB in solution was almost completely adsorbed by the GO nanosheets (compare the experimental data with the dotted line representing the bisector of the graph, corresponding to 100% of MB adsorbed on GO). On the other hand, when MB/GO > 1, a fraction of the MB remains in solution. With increasing the total MB/GO ratio, the aliquot of MB remaining in solution increased,

suggesting an asymptotic behavior for MB adsorption. This was confirmed by the calculation of the sorption isotherm (Figure 3c), which showed a Langmuirian trend:

$$S_{MB} = \frac{\beta \cdot S_{MB,max} \cdot C_{MB,free}}{1 + S_{MB,max} \cdot C_{MB,free}} \qquad \text{(eq. 2)}$$

where $S_{MB,max}$ is the saturation concentration (1.63 mg /mg) and β = 2.0 L/mg.

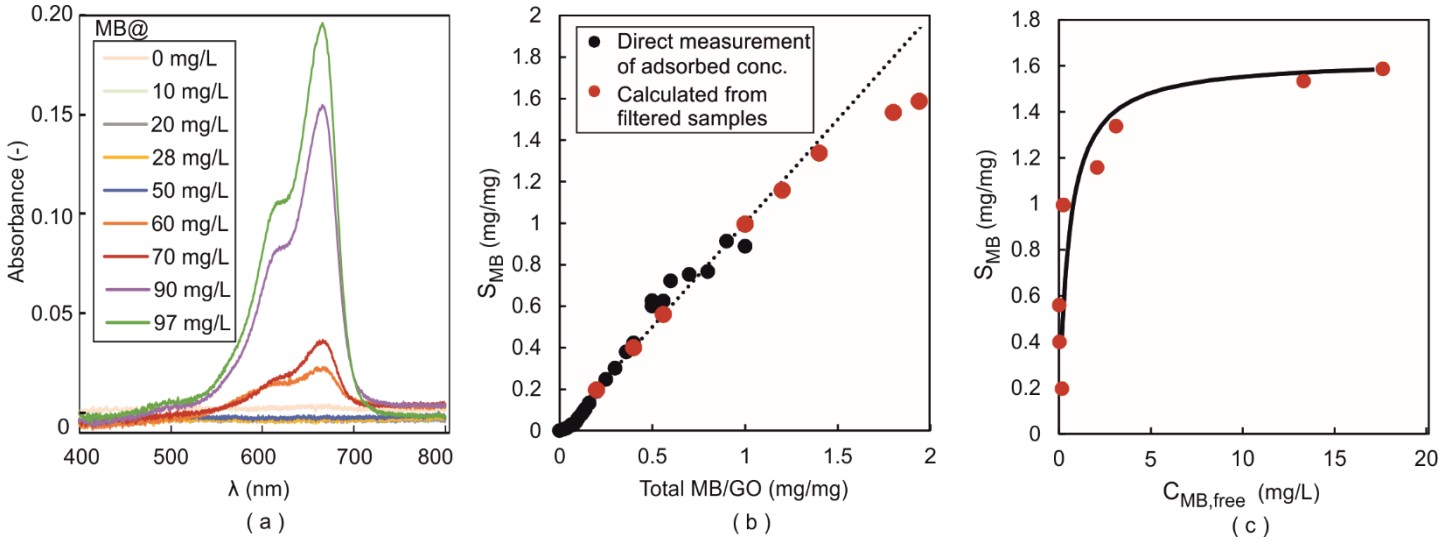

Figure 3: Adsorption tests for C_{GO} = 50 mg/L: (a) UV-vis spectra of filtered samples at different concentrations of MB. (b) Mass concentration of adsorbed MB (S_{MB}) vs total (initially dosed) MB/GO ratio calculated from UV-vis spectra of the suspension using eq. 1 (black points) and obtained from the measurement of free MB concentration in filtered samples (red points); the bisector is reported as dotted line for comparison with experimental data. (c) Adsorption isotherm: measured concentrations (red points) and fitted Langmuir model (black line).

3.3. Column tests: co-transport and retention of MB-loaded GO nanosheets

Batch and column transport pre-tests were performed for GO-free MB solutions to assess the interaction between MB and silica sand. A GO-free MB solution ($C_{0,MB}$ = 25 mg/L, NaCl 20 mM, pH = 8.5 adjusted by NaOH addition) was injected into a saturated sand column for 19 pore volumes (PVs), and then flushed with the same MB-free electrolyte solution (Figure 4a). As expected, the positively charged MB molecules showed a high affinity to the negatively charged sand grains (Zeta potential: -38.2 ± 2 mV) resulting in a delayed breakthrough at

approximately 10 PVs after injection, and a retardation factor of 14. This behavior corresponds to a reversible adsorption of MB. The sorption isotherm in the same electrolyte solution determined in batch evidenced a Langmuirian shape (Figure 4b). Conversely, batch tests performed putting in contact MB-loaded sand grains with MB-free DIw showed a complete and irreversible adsorption, with no release of MB (data not reported), due to the stronger affinity of MB cations to the sand surface in DI water (Zeta potential: -74.0 ± 2 mV).

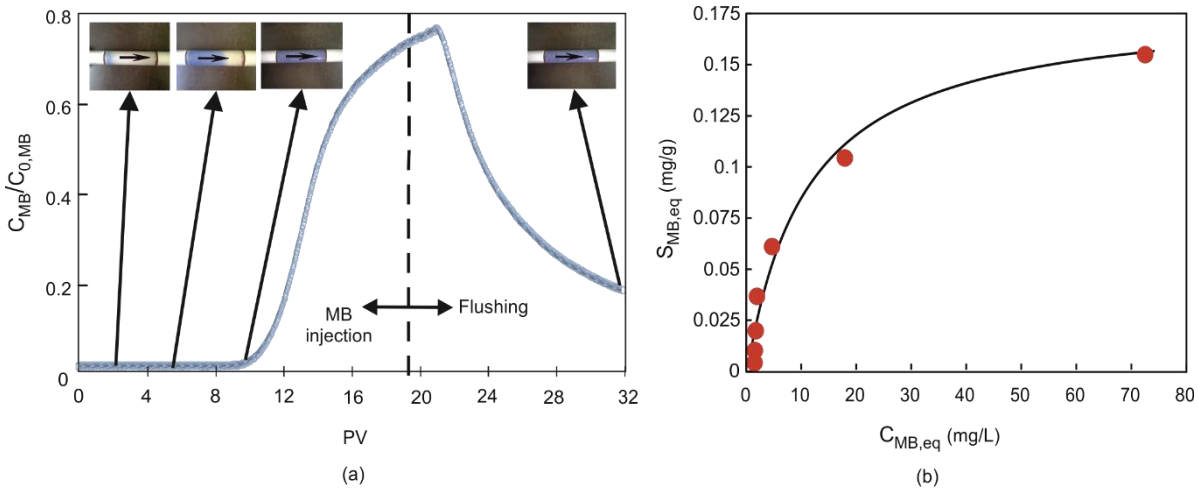

Figure 4: (a) Breakthrough curve of methylene blue ($C_{0,MB}$ = 25 mg/L, NaCl 20 mM, same flow rate as GO tests) injected in a sand-packed column for 19 pore volumes, followed by flushing (NaCl 20 mM). The concentration of dissolved MB at column inlet and outlet was monitored in-line at λ = 678 nm. (b) Batch adsorption isotherm for MB in contact with silica sand, (NaCl 20 mM, T = 20°C). $C_{MB,eq}$ = concentration in water phase at equilibrium, $S_{MB,eq}$ = concentration in solid phase at equilibrium. The red dots represent the experimental data, the black curve is a Langmuir isotherm $S_{MB,eq} = \alpha \cdot \beta \cdot C_{MB,eq} / (1 + \alpha \cdot C_{MB,eq})$, where α = 0.09 L/mg, β = 0.18.

Column co-transport tests of MB-loaded GO nanosheets were then performed at $C_{0,GO}$ = 50 mg/L and $C_{0,MB}$ = 0 to 30 mg/L. The GO and MB concentrations were selected based on the results of batch tests, in order to explore a wide range of GO colloidal stability, but always in the absence of free MB. Full spectra were collected every 30 s at the column inflow and outflow. Breakthrough curves of GO nanosheets and adsorbed MB (C_{GO} and $C_{MB,ads}$) were

calculated from Eq.1 and are reported in Figure 5. No freely dissolved MB was detected at the column outlet in any co-transport test and hence, for the sake of simplicity, the concentration of MB adsorbed on GO, detected at column inlet/outlet, are hereby indicated as $C_{0,MB}$ and C_{MB}, respectively, instead of $C_{0,MB,ads}$ and $C_{MB,ads}$.

The breakthrough curves (BTCs) of GO nanosheets at different MB concentrations (Figure 5a) showed, during injection, a plateau $C_{GO}/C_{0,GO}$ approximately equal to 1 for MB concentration up to 10 g/L, and lower, but still significant, for $C_{0,MB}$ = 20 mg/L. Conversely, for $C_{0,MB}$ = 30 mg/L an almost negligible GO breakthrough was observed. This behavior is coherent with the colloidal stability and the particle Zeta potential of GO nanosheets observed in the inlet suspension and in batch tests for $C_{0,GO}$ = 50 mg/L (*Table 1* and Figure S1). For MB concentration up to 10 mg/L the GO nanosheets were stably dispersed, and no aggregation was observed in the inlet reservoir. The Zeta potential was equal to -50±4 mV and -40.8±2 mV for C_{MB} = 0 mg/L and 10 mg/L, respectively. In these conditions the GO nanosheets travelled (almost) undisturbed through the porous medium, reaching $C_{GO}/C_{0,GO}$ = 1 at column outflow. Conversely, for $C_{0,MB}$ = 20 mg/L slight aggregation was observed in the inlet reservoir, coherently with the batch tests and the measured zeta potential (-21.3±2 mV), along with a more limited mobility. More specifically, the shape of the breakthrough curve indicates a mechanical filtration of partly aggregated GO nanosheets (this is suggested by the plateau $C_{GO}/C_{0,GO} < 1$) with limited ripening on the late stages (see the slightly declining BTC after 5 PVs). For $C_{0,MB}$ = 30 mg/L, aggregation had a major impact, in agreement with the Zeta potential close to neutrality (-6.6±2 mV), and resulted in mechanical filtration of the flocs in the column and consequently in a negligible breakthrough of the GO nanosheets.

The flushing performed with NaCl 20 mM at pH=8.5 led to a limited tailing for all tests, indicating that detachment was a minor phenomenon even in those tests where the previous deposition was not negligible. For all tests the mass recovery at the end of the flushing was

higher than 70%, except for $C_{0,MB}$ = 30 mg/L, for which a GO recovery of 61.47% was registered (*Table 1*).

Table 1: Mass balance for GO and MB in column co-transport tests: concentrations of GO and MB injected at column inlet ($C_{0,GO}$ and $C_{0,MB}$) and corresponding inlet mass ratio MB/GO, and mass balances for GO and MB expressed as percentage of GO or MB recovered at column outlet with respect to the injected ones, after the flushing step. The outflow mass ratio at column outlet averaged over the entire column test ($MB/GO\,|_{out}$) was calculated from Eq. 3.

Column inlet				**Column outlet**		
Injected GO conc. $C_{0,GO}$ (mg/L)	**Injected MB conc. $C_{0,MB}$ (mg/L)**	**$MB/GO\,|_{in}$ (mass ratio) (-)**	**Colloidal stability during the injection**	**Eluted GO after flushing (%)**	**Eluted MB after flushing (%)**	**$MB/GO\,|_{out}$ (mass ratio) (-)**
50	30	0.60	Relatively Aggregated	2.62	0.57	0.131
50	20	0.40	Relatively Aggregated	70.84	44.76	0.253
50	10	0.20	Stable	91.63	65.49	0.143
50	5	0.10	Stable	92.62	76.57	0.083
50	2	0.04	Stable	92.88	93.47	0.040
50	0	--	Stable	93.86	-	-

MB breakthrough decreased with increasing MB/GO ratio at column inlet (Figure 5b). Noticeably, the BTCs and associated mass balances of adsorbed MB do not entirely reflect the GO BTCs. The adsorbed MB showed lower breakthrough concentrations compared to GO nanosheets in the corresponding column test. This phenomenon is further evidenced in Figure 6, where the MB/GO ratio at column outlet is reported for two selected tests ($C_{0,MB}$ = 10 and 20 mg/L, corresponding respectively to MB/GO inlet ratio of 0.2 and 0.4). During both tests, the MB/GO ratio at the column outlet remained always significantly below the inlet value, even though a slight increase can be observed over time, particularly for the test at $C_{0,MB}$ = 10 mg/L. This finding suggests that a fraction of the MB initially adsorbed onto GO nanosheets desorbed from it while flowing through the column and competitively attached onto the sand grains. The observation of light blue shades on the sand grains within the column at the end of the tests was a visual evidence for this.

The discrepancy between inlet and outlet mass ratios was quantified also from the mass balances for GO and MB (*Table 1*). To this aim, the recovered mass ratio of MB to GO at column outlet ($MB/GO|_{out}$), was calculated as:

$$MB/GO|_{out} = \frac{\int_{t=0}^{t_{end}} C_{MB} dt}{\int_{t=0}^{t_{end}} C_{GO} dt} \qquad \text{(eq. 3)}$$

where t_{end} is the time corresponding to the end of the flushing.

The discrepancy between the nominal MB/GO mass ratio injected in the column ($MB/GO\,|_{in}$) and the ratio of recovered masses at column outlet ($MB/GO\,|_{out}$) is more pronounced at higher injected MB doses. Significant discrepancies were observed in particular for $C_{0,MB} \geq 10$ mg/L.

The more pronounced desorption of MB from GO nanosheets (and adsorption onto sand grains) observed for higher MB/GO inlet ratios can be attributed to differences in the affinity of MB to sand and GO surface depending on the inlet MB/GO itself: for $C_{0,MB} \leq 10$ mg/L, the higher negative surface charge of GOs (zeta potential -50±4 mV) compared to sand (38.2±2 mV) likely lead to a stronger electrostatic interaction force of MB with GO compared to the sand grains. Literature studies on MB adsorption by quartz sand with different grain zeta potentials showed that the adsorption efficiency decreases with decreasing sand surface charge [73-75].

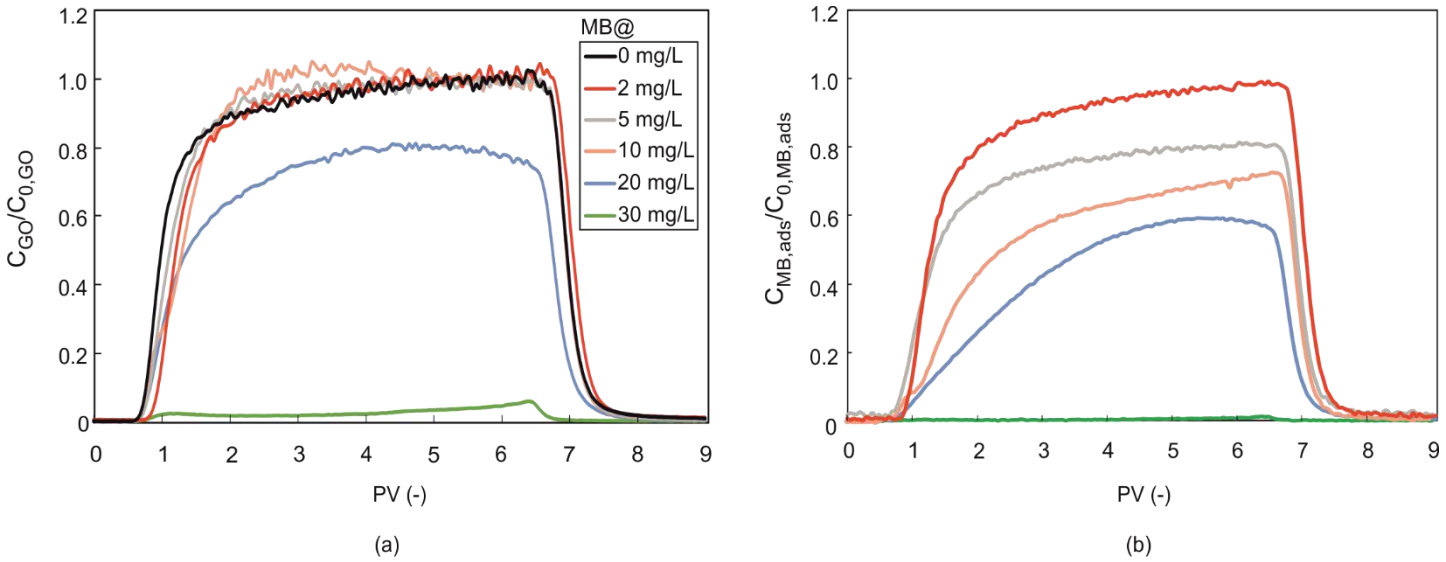

Figure 5: Co-transport tests: measured normalized breakthrough curves (BTCs) for (a) GO nanosheets (C_{GO} = outlet concentration, $C_{0,GO}$ = inlet concentration) and (b) adsorbed MB, reported as a function of the number of injected pore volumes (PVs). Tests were performed injecting $C_{0,GO}$=50 mg/L and different MB concentrations. Darcy velocity: $8.1 \cdot 10^{-5}$ m/s.

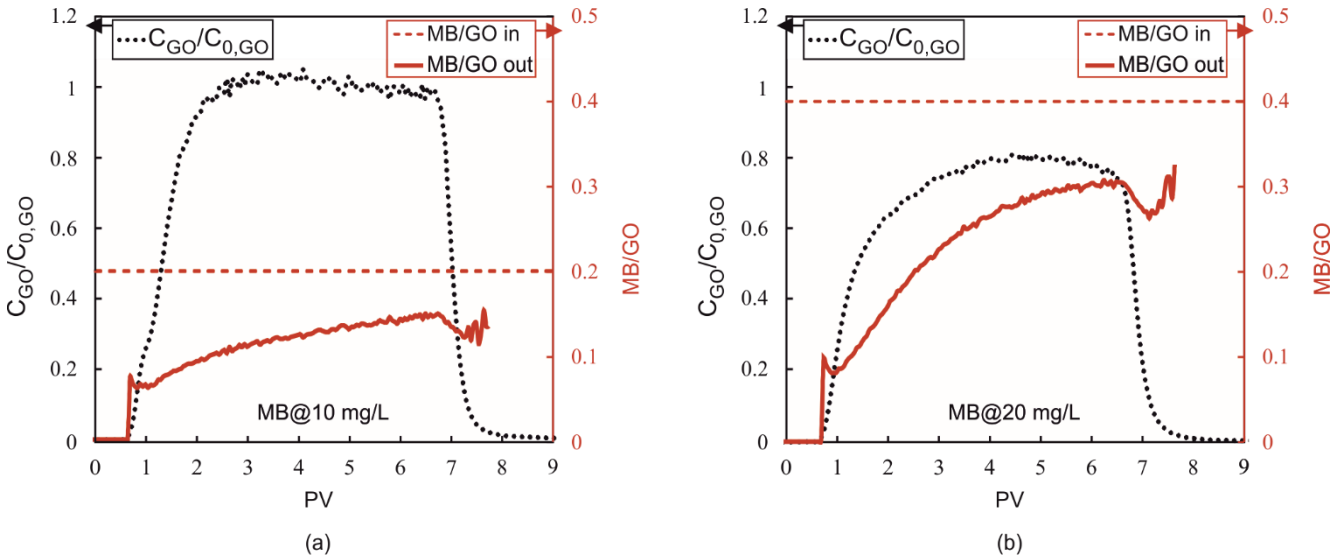

Figure 6: Co-transport tests: MB/GO ratio at column inlet (dashed lines) and outlet (continuous lines) as a function of injected pore volumes (PV) for transport tests performed injecting $C_{0,GO}$ = 50 mg/L with (a) $C_{0,MB,ads}$ = 20 mg/L and (b) 10 mg/L. The corresponding GO breakthrough curves (dotted lines) are also reported to improve readability of the graph. MB/GO ratio is calculated for C_{GO}>1 mg/L to discard poorly significant data.

3.4. Removal of MB adsorbed on sand by GO

The GO capability to remove MB adsorbed on sand grains was assessed in a set of column tests mimicking, in simplified conditions, the possible steps of an aquifer contamination and decontamination process (Figure 7). In all tests, the sand-packed column was first contaminated injecting a MB solution (20 mg/L, pH = 8.5) for 26 PVs. MB breakthrough was observed after approximately 10 PVs. After 26 PVs, $C_{MB}/C_{0,MB} \approx 0.8$ was reached at the outlet, corresponding to an average concentration of adsorbed MB of 0.15 mg/g in the column. During flushing #1, performed injecting the NaCl 20 mM solution, the flow of MB-free groundwater through the contaminated area was mimicked. In this step, slow MB desorption occurred, coherently with the reversible adsorption previously observed in batch and column tests. The flushing #2, conversely, mimicked the effects of the injection of a washing solution (DIw) or a washing GO dispersion ($C_{0,GO}$ = 50 mg/L, dispersed in NaCl 20 mM or DIw). To elucidate the role of the tested washing solutions/suspensions on MB release, beside breakthrough curves, also mass balances for flushing #2 (Table 2 and bottom part of Figure 7) were calculated.

When GO in the NaCl solution was injected for column flushing, no clear release of MB was observed: this suggests that, at this salt concentration, the MB molecule has a stronger affinity to sand grains rather than to GO nanosheets. Also DIw (without GO) proved not suitable as a washing solution: in this test the MB recovery at column outflow dropped abruptly as soon as DIw is injected, and only 8.4% of the MB remained adsorbed on the sand was released during flushing #2. This is coherent with the negligible desorption of MB observed in batch tests for MB-loaded sand in contact with DIw due to the very strong affinity of MB cations to the highly negative surface of the sand, as discussed above.

Conversely, the injection of GO dispersed in DIw gave rise to a strong MB release peak immediately after GO injection: in 3 PVs, 25.8% of the remaining MB was collected at the

outflow. After the peak, a declining MB recovery was observed, and the breakthrough curve collapsed on the BTC obtained for GO in the NaCl solution. This behavior can be attributed to the strongly negative surface of GO nanosheets dispersed in DIw (Zeta potential: -57.1 ± 3 mV), which can partly desorb MB molecules from the sand surface and wash them out of the column. Based on these results, the GO-DIw could therefore be useful in the perspective of an accelerated clean-up of a contamination source in remediation applications.

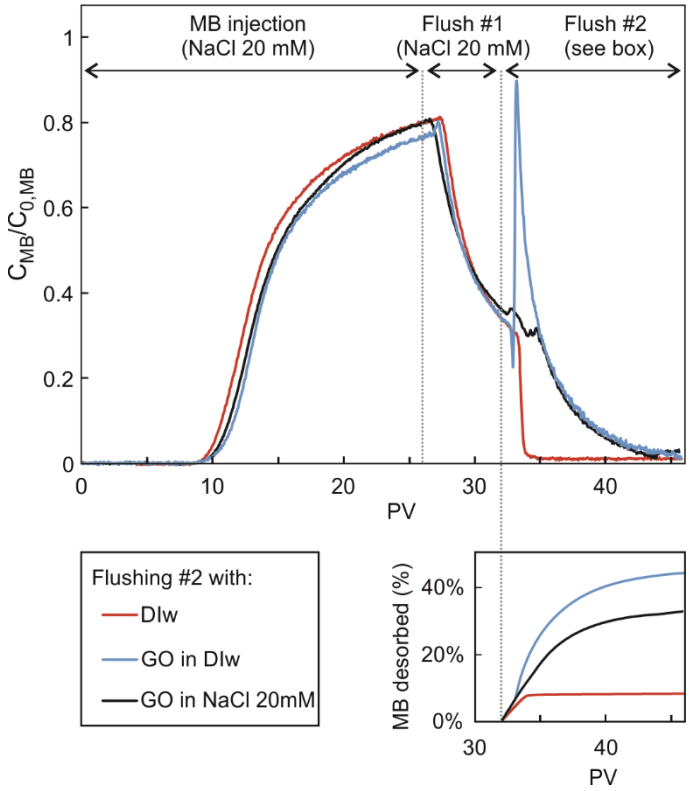

Figure 7: Breakthrough curves of total (free + adsorbed) methylene blue in release tests. 1-26 PVs: MB injection (25 mg/L) in NaCl 20 mM; 27-32 PVs: flushing #1 with NaCl 20 mM; 33-46 PVs: flushing #2 with the washing solution/dispersion (as detailed in the legend). Darcy velocity: $8.1 \cdot 10^{-5}$ m/s. The bottom graph reports the percentage of MB mass released starting at 32 PVs with respect to the mass of MB retained in the column at beginning of flushing #2.

Table 2: Methylene blue release tests: mass balance for MB released during flushing #2. The percentages are calculated with respect to the mass of MB retained in the column at the beginning of flushing #2.

		Flushing #2 with		
		DIw	**GO in DIw**	**GO in NaCl 20 mM**
% MB desorbed @	32 PVs	0.0%	0.0%	0.0%
	35 PVs	8.1%	25.8%	17.3%
	38 PVs	8.2%	36.9%	26.9%
	42 PVs	8.3%	42.4%	31.2%
	46 PVs	8.4%	44.4%	32.9%

4. Conclusions

This study showed that GO nanosheets have a high mobility in porous media, a strong capacity to absorb environmentally relevant compounds, and a good potential to facilitate their removal when adsorbed on the porous medium. The batch experiments demonstrated that GO is highly effective in the rapid adsorption of MB, hereby chosen as a model contaminant representative of a broader set of cationic pollutants. Even though the sorption capacity is not unlimited, in the tested conditions the maximum loading was higher than 1.5 mg/mg, which represents an extremely interesting removal efficiency in view of a technical application in water purification.

Methylene blue itself is prone to strong adsorption onto negatively charged granular media (e.g. the silica sand used in this study, and more in general in soils and aquifer systems) due to the high affinity of MB cations with the negatively charged surface of the sand. However, when co-transported with GO, its mobility is dramatically enhanced. Batch sorption and colloidal stability tests showed that, under the tested conditions (i.e. pH>8.5 and NaCl 20 mM), the colloidal stability of MB-loaded GO depends on the ionic strength and on the MB/GO ratio, which both directly affect colloidal stability, aggregate size and ultimately transport in the porous medium of the MB-loaded GO nanosheets. The co-transport results

revealed that the MB-loaded GO nanosheets with an initial MB/GO ratio lower than 0.5 maintained a good colloidal stability and were transported through the porous medium without significant retention. On the other hand, MB-loaded GO nanosheets with a higher ratio aggregated over time and were filtered in the columns. These findings give important indications on the expected mobility of GO nanosheets at the field scale, even though further studies at larger scales are undoubtedly needed to extrapolate relevant behaviors observed in column tests.

The desorption experiments, aimed at testing the capability of different washing solutions/suspensions to accelerate the removal of MB from contaminated sand, showed a high potential of GO nanosheets in this sense. The major positive effect was a significantly accelerated desorption, thus opening positive perspectives for the potential application of GO for groundwater reclamation purposes. In particular, a GO-assisted soil flushing can be envisioned. In this way, fast desorption of contaminants strongly adsorbed on the aquifer solid matrix can be promoted, thus allowing for the treatment of secondary sources of contamination.

It is finally worth to highlight that the experiments herein presented were conducted in simplified conditions, namely using clean silica sand and a solution of NaCl. The results evidenced the strong impact of the ionic strength on the MB desorption and removal, suggesting that pore water composition and more in general other hydrochemical parameters would likely have a significant impact on the co-transport of GO and cationic contaminants in more complex scenarios. Consequently, the results of this study are intended as a preliminary step toward the development of a novel GO-based soil flushing approach, and further investigation is needed to elucidate controlling mechanisms and key design parameters in case this approach is developed at a larger scale.

Acknowledgements

The authors are grateful to prof. Barbara Bonelli and Dr. Roberto Nasi (DISAT – Politecnico di Torino) for the support in FT-IR analysis and interpretation and to Leonardo Magherini and Monica Granetto for the support in laboratory experiments. The authors also wish to thank Valentina Quaranta and Sofia Credaro for their support in preparing the manuscript.

Funding

This research did not receive any specific grant from funding agencies in the public, commercial, or not-for-profit sectors.

Cited literature

[1] G. Zhao, J. Li, X. Ren, C. Chen, X. Wang, Few-Layered Graphene Oxide Nanosheets As Superior Sorbents for Heavy Metal Ion Pollution Management, Environmental Science & Technology, 45 (2011) 10454-10462.
[2] J. Zhao, W. Ren, H.-M. Cheng, Graphene sponge for efficient and repeatable adsorption and desorption of water contaminations, Journal of Materials Chemistry, 22 (2012) 20197-20202.
[3] S. Chowdhury, R. Balasubramanian, Recent advances in the use of graphene-family nanoadsorbents for removal of toxic pollutants from wastewater, Advances in Colloid and Interface Science, 204 (2014) 35-56.
[4] X. Huang, Z. Yin, S. Wu, X. Qi, Q. He, Q. Zhang, Q. Yan, F. Boey, H. Zhang, Graphene-based materials: Synthesis, characterization, properties, and applications, Small, 7 (2011) 1876-1902.
[5] J. Liu, L. Cui, D. Losic, Graphene and graphene oxide as new nanocarriers for drug delivery applications, Acta Biomaterialia, 9 (2013) 9243-9257.
[6] Z. Qi, L. Zhang, W. Chen, Transport of graphene oxide nanoparticles in saturated sandy soil, Environmental Sciences: Processes and Impacts, 16 (2014) 2268-2277.
[7] R. Hosseinzadeh, K. Khorsandi, G. Hosseinzadeh, Graphene oxide-methylene blue nanocomposite in photodynamic therapy of human breast cancer, Journal of Biomolecular Structure and Dynamics, 36 (2018) 2216-2223.

[8] A. Sahu, W.I. Choi, J.H. Lee, G. Tae, Graphene oxide mediated delivery of methylene blue for combined photodynamic and photothermal therapy, Biomaterials, 34 (2013) 6239-6248.
[9] M. Wojtoniszak, D. Rogińska, B. Machaliński, M. Drozdzik, E. Mijowska, Graphene oxide functionalized with methylene blue and its performance in singlet oxygen generation, Materials Research Bulletin, 48 (2013) 2636-2639.
[10] K. Yang, L. Hu, X. Ma, S. Ye, L. Cheng, X. Shi, C. Li, Y. Li, Z. Liu, Multimodal imaging guided photothermal therapy using functionalized graphene nanosheets anchored with magnetic nanoparticles, Advanced Materials, 24 (2012) 1868-1872.
[11] X. Yang, Y. Wang, X. Huang, Y. Ma, Y. Huang, R. Yang, H. Duan, Y. Chen, Multi-functionalized graphene oxide based anticancer drug-carrier with dual-targeting function and pH-sensitivity, Journal of Materials Chemistry, 21 (2011) 3448-3454.
[12] L. Zhang, J. Xia, Q. Zhao, L. Liu, Z. Zhang, Functional graphene oxide as a nanocarrier for controlled loading and targeted delivery of mixed anticancer drugs, Small, 6 (2010) 537-544.
[13] S.C. Smith, D.F. Rodrigues, Carbon-based nanomaterials for removal of chemical and biological contaminants from water: A review of mechanisms and applications, Carbon, 91 (2015) 122-143.
[14] I. Ali, A.A. Basheer, X.Y. Mbianda, A. Burakov, E. Galunin, I. Burakova, E. Mkrtchyan, A. Tkachev, V. Grachev, Graphene based adsorbents for remediation of noxious pollutants from wastewater, Environment International, 127 (2019) 160-180.
[15] Z. Ding, X. Hu, V.L. Morales, B. Gao, Filtration and transport of heavy metals in graphene oxide enabled sand columns, Chemical Engineering Journal, 257 (2014) 248-252.
[16] J.L. Gong, Y.L. Zhang, Y. Jiang, G.M. Zeng, Z.H. Cui, K. Liu, C.H. Deng, Q.Y. Niu, J.H. Deng, S.Y. Huan, Continuous adsorption of Pb(II) and methylene blue by engineered graphite oxide coated sand in fixed-bed column, Applied Surface Science, 330 (2015) 148-157.
[17] A. Gopalakrishnan, R. Krishnan, S. Thangavel, G. Venugopal, S.J. Kim, Removal of heavy metal ions from pharma-effluents using graphene-oxide nanosorbents and study of their adsorption kinetics, Journal of Industrial and Engineering Chemistry, 30 (2015) 14-19.
[18] C.H. Chia, N.F. Razali, M.S. Sajab, S. Zakaria, N.M. Huang, H.N. Lim, Methylene Blue Adsorption on Graphene Oxide, Sains Malaysiana, 42 (2013) 819-826.
[19] Z. Hosseinabadi-Farahani, H. Hosseini-Monfared, N.M. Mahmoodi, Graphene oxide nanosheet: preparation and dye removal from binary system colored wastewater, Desalination and Water Treatment, 56 (2015) 2382-2394.
[20] S. Sohni, K. Gul, F. Ahmad, I. Ahmad, A. Khan, N. Khan, S.B. Khan, Highly efficient removal of acid red-17 and bromophenol blue dyes from industrial wastewater using graphene oxide functionalized magnetic chitosan, Polymer Composites, 39 (2018) 3317-3328.
[21] D. Wang, L. Liu, X. Jiang, J. Yu, X. Chen, Adsorption and removal of malachite green from aqueous solution using magnetic β-cyclodextrin-graphene oxide

nanocomposites as adsorbents, Colloids and Surfaces A: Physicochemical and Engineering Aspects, 466 (2015) 166-173.
[22] L.A. Al-Khateeb, W. Hakami, M.A. Salam, Removal of non-steroidal anti-inflammatory drugs from water using high surface area nanographene: Kinetic and thermodynamic studies, Journal of Molecular Liquids, 241 (2017) 733-741.
[23] P. Banerjee, P. Das, A. Zaman, P. Das, Application of graphene oxide nanoplatelets for adsorption of Ibuprofen from aqueous solutions: Evaluation of process kinetics and thermodynamics, Process Safety and Environmental Protection, 101 (2016) 45-53.
[24] V. Kumar Gupta, S. Agarwal, M. Asif, A. Fakhri, N. Sadeghi, Application of response surface methodology to optimize the adsorption performance of a magnetic graphene oxide nanocomposite adsorbent for removal of methadone from the environment, Journal of Colloid and Interface Science, 497 (2017) 193-200.
[25] M.T. Yagub, T.K. Sen, S. Afroze, H.M. Ang, Dye and its removal from aqueous solution by adsorption: A review, Advances in Colloid and Interface Science, 209 (2014) 172-184.
[26] P. Janoš, H. Buchtová, M. Rýznarová, Sorption of dyes from aqueous solutions onto fly ash, Water Research, 37 (2003) 4938-4944.
[27] K. Rastogi, J.N. Sahu, B.C. Meikap, M.N. Biswas, Removal of methylene blue from wastewater using fly ash as an adsorbent by hydrocyclone, Journal of Hazardous Materials, 158 (2008) 531-540.
[28] M.A.M. Khraisheh, M.S. Alg-Houti, Enhanced Dye Adsorption by Microemulsion-Modified Calcined Diatomite (μE-CD), Adsorption, 11 (2005) 547-559.
[29] M.J. Iqbal, M.N. Ashiq, Adsorption of dyes from aqueous solutions on activated charcoal, Journal of Hazardous Materials, 139 (2007) 57-66.
[30] X. He, K.B. Male, P.N. Nesterenko, D. Brabazon, B. Paull, J.H.T. Luong, Adsorption and desorption of methylene blue on porous carbon monoliths and nanocrystalline cellulose, ACS Applied Materials and Interfaces, 5 (2013) 8796-8804.
[31] L. Wu, L. Liu, B. Gao, R. Muñoz-Carpena, M. Zhang, H. Chen, Z. Zhou, H. Wang, Aggregation kinetics of graphene oxides in aqueous solutions: Experiments, mechanisms, and modeling, Langmuir, 29 (2013) 15174-15181.
[32] G.K. Ramesha, A. Vijaya Kumara, H.B. Muralidhara, S. Sampath, Graphene and graphene oxide as effective adsorbents toward anionic and cationic dyes, Journal of Colloid and Interface Science, 361 (2011) 270-277.
[33] S.T. Yang, S. Chen, Y. Chang, A. Cao, Y. Liu, H. Wang, Removal of methylene blue from aqueous solution by graphene oxide, Journal of Colloid and Interface Science, 359 (2011) 24-29.
[34] R. Allgayer, N. Yousefi, N. Tufenkji, Graphene oxide sponge as adsorbent for organic contaminants: comparison with granular activated carbon and influence of water chemistry, Environmental Science: Nano, 7 (2020) 2669-2680.
[35] N. Yousefi, K.K.W. Wong, Z. Hosseinidoust, H.O. Sørensen, S. Bruns, Y. Zheng, N. Tufenkji, Hierarchically porous, ultra-strong reduced graphene oxide-cellulose nanocrystal sponges for exceptional adsorption of water contaminants, Nanoscale, 10 (2018) 7171-7184.

[36] L. Bai, Z. Li, Y. Zhang, T. Wang, R. Lu, W. Zhou, H. Gao, S. Zhang, Synthesis of water-dispersible graphene-modified magnetic polypyrrole nanocomposite and its ability to efficiently adsorb methylene blue from aqueous solution, Chemical Engineering Journal, 279 (2015) 757-766.
[37] L. Ai, C. Zhang, Z. Chen, Removal of methylene blue from aqueous solution by a solvothermal-synthesized graphene/magnetite composite, Journal of Hazardous Materials, 192 (2011) 1515-1524.
[38] J.-H. Deng, X.-R. Zhang, G.-M. Zeng, J.-L. Gong, Q.-Y. Niu, J. Liang, Simultaneous removal of Cd(II) and ionic dyes from aqueous solution using magnetic graphene oxide nanocomposite as an adsorbent, Chemical Engineering Journal, 226 (2013) 189-200.
[39] S. Ghorai, A. Sarkar, M. Raoufi, A.B. Panda, H. Schönherr, S. Pal, Enhanced Removal of Methylene Blue and Methyl Violet Dyes from Aqueous Solution Using a Nanocomposite of Hydrolyzed Polyacrylamide Grafted Xanthan Gum and Incorporated Nanosilica, ACS Applied Materials & Interfaces, 6 (2014) 4766-4777.
[40] A.A. Nayl, A.I. Abd-Elhamid, A.A. El-Shanshory, H.M.A. Soliman, E.-R. Kenawy, H.F. Aly, Development of sponge/graphene oxide composite as eco-friendly filter to remove methylene blue from aqueous media, Applied Surface Science, 496 (2019) 143676.
[41] A. Kovtun, E. Campodoni, L. Favaretto, M. Zambianchi, A. Salatino, S. Amalfitano, M.L. Navacchia, B. Casentini, V. Palermo, M. Sandri, M. Melucci, Multifunctional graphene oxide/biopolymer composite aerogels for microcontaminants removal from drinking water, Chemosphere, 259 (2020) 127501.
[42] Y. Li, X. Zhang, A. Yang, C. Jiang, G. Zhang, J. Mao, Q. Meng, Polyphenol etched ZIF-8 modified graphene oxide nanofiltration membrane for efficient removal of salts and organic molecules, Journal of Membrane Science, 635 (2021) 119521.
[43] L. Feriancikova, S. Xu, Deposition and remobilization of graphene oxide within saturated sand packs, Journal of Hazardous Materials, 235-236 (2012) 194-200.
[44] L. Liu, B. Gao, L. Wu, V.L. Morales, L. Yang, Z. Zhou, H. Wang, Deposition and transport of graphene oxide in saturated and unsaturated porous media, Chemical Engineering Journal, 229 (2013) 444-449.
[45] Y. Sun, B. Gao, S.A. Bradford, L. Wu, H. Chen, X. Shi, J. Wu, Transport, retention, and size perturbation of graphene oxide in saturated porous media: Effects of input concentration and grain size, Water Research, 68 (2015) 24-33.
[46] C. Bianco, T. Tosco, R. Sethi, A 3-dimensional micro- and nanoparticle transport and filtration model (MNM3D) applied to the migration of carbon-based nanomaterials in porous media, Journal of Contaminant Hydrology, 193 (2016) 10-20.
[47] A. Beryani, M.R. Alavi Moghaddam, T. Tosco, C. Bianco, S.M. Hosseini, E. Kowsari, R. Sethi, Key factors affecting graphene oxide transport in saturated porous media, Science of The Total Environment, 698 (2020) 134224.
[48] J.D. Lanphere, C.J. Luth, S.L. Walker, Effects of Solution Chemistry on the Transport of Graphene Oxide in Saturated Porous Media, Environmental Science & Technology, 47 (2013) 4255-4261.
[49] Z. Qi, L. Zhang, F. Wang, L. Hou, W. Chen, Factors controlling transport of graphene oxide nanoparticles in saturated sand column, 33 (2014) 998-1004.

[50] C. Chen, J. Shang, X. Zheng, K. Zhao, C. Yan, P. Sharma, K. Liu, Effect of physicochemical factors on transport and retention of graphene oxide in saturated media, Environmental Pollution, 236 (2018) 168-176.
[51] V.I. Syngouna, G.I. Giannadakis, C.V. Chrysikopoulos, Interaction of graphene oxide nanoparticles with quartz sand and montmorillonite colloids, Environmental Technology, 41 (2020) 1127-1138.
[52] S. Mondal, M.K. Purkait, S. De, Advances in dye removal technologies, 1 ed., Springer Nature, Singapore, 2018.
[53] M. Rafatullah, O. Sulaiman, R. Hashim, A. Ahmad, Adsorption of methylene blue on low-cost adsorbents: A review, Journal of Hazardous Materials, 177 (2010) 70-80.
[54] Y. Li, Q. Du, T. Liu, X. Peng, J. Wang, J. Sun, Y. Wang, S. Wu, Z. Wang, Y. Xia, L. Xia, Comparative study of methylene blue dye adsorption onto activated carbon, graphene oxide, and carbon nanotubes, Chemical Engineering Research and Design, 91 (2013) 361-368.
[55] W. Zhang, C. Zhou, W. Zhou, A. Lei, Q. Zhang, Q. Wan, B. Zou, Fast and considerable adsorption of methylene blue dye onto graphene oxide, Bulletin of Environmental Contamination and Toxicology, 87 (2011) 86-90.
[56] Y. Jiang, X. Zhang, X. Yin, H. Sun, N. Wang, Graphene oxide-facilitated transport of Pb2+and Cd2+in saturated porous media, Science of the Total Environment, 631-632 (2018) 369-376.
[57] X. Yin, Y. Jiang, Y. Tan, X. Meng, H. Sun, N. Wang, Co-transport of graphene oxide and heavy metal ions in surface-modified porous media, Chemosphere, 218 (2019) 1-13.
[58] K. Zhao, C. Chen, T. Cheng, J. Shang, Graphene oxide-facilitated uranium transport and release in saturated medium : Effect of ionic strength and medium structure, Environmental Pollution, 247 (2019) 668-677.
[59] D.D. Zhou, X.H. Jiang, Y. Lu, W. Fan, M.X. Huo, J.C. Crittenden, Cotransport of graphene oxide and Cu(II) through saturated porous media, Science of the Total Environment, 550 (2016) 717-726.
[60] Z. Chi, Y. Zhu, W. Liu, H. Huang, H. Li, Selective removal of As(III) using magnetic graphene oxide ion-imprinted polymer in porous media: Potential effect of external magnetic field, Journal of Environmental Chemical Engineering, 9 (2021) 105671.
[61] M.P. Georgopoulou, V.I. Syngouna, C.V. Chrysikopoulos, Influence of graphene oxide nanoparticles on the transport and cotransport of biocolloids in saturated porous media, Colloids and Surfaces B: Biointerfaces, 189 (2020) 110841.
[62] C.V. Chrysikopoulos, N.P. Sotirelis, N.G. Kallithrakas-Kontos, Cotransport of Graphene Oxide Nanoparticles and Kaolinite Colloids in Porous Media, Transport in Porous Media, 119 (2017) 181-204.
[63] D. Pakulski, W. Czepa, S. Witomska, A. Aliprandi, P. Pawluć, V. Patroniak, A. Ciesielski, P. Samorì, Graphene oxide-branched polyethylenimine foams for efficient removal of toxic cations from water, Journal of Materials Chemistry A, 6 (2018) 9384-9390.
[64] P.R. Johnson, N. Sun, M. Elimelech, Colloid transport in physically and geochemically heterogeneous porous media. Modeling, measurements, and

parameter identification, Environmental Science and Technology, 30 (1996) 3284-3293.
[65] M. Lotya, A. Rakovich, J.F. Donegan, J.N. Coleman, Measuring the lateral size of liquid-exfoliated nanosheets with dynamic light scattering, Nanotechnology, 24 (2013) 265703.
[66] T. Tosco, J. Bosch, R.U. Meckenstock, R. Sethi, Transport of ferrihydrite nanoparticles in saturated porous media: Role of ionic strength and flow rate, Environmental Science and Technology, 46 (2012) 4008-4015.
[67] F. Mondino, A. Piscitello, C. Bianco, A. Gallo, A. de Folly D'Auris, T. Tosco, M. Tagliabue, R. Sethi, Injection of Zerovalent Iron Gels for Aquifer Nanoremediation: Lab Experiments and Modeling, Water, 12 (2020) 826.
[68] P. Sharma, M.R. Das, Removal of a cationic dye from aqueous solution using graphene oxide nanosheets: Investigation of adsorption parameters, Journal of Chemical and Engineering Data, 58 (2013) 151-158.
[69] O.V. Ovchinnikov, A.V. Evtukhova, T.S. Kondratenko, M.S. Smirnov, V.Y. Khokhlov, O.V. Erina, Manifestation of intermolecular interactions in FTIR spectra of methylene blue molecules, Vibrational Spectroscopy, 86 (2016) 181-189.
[70] K. Haubner, J. Murawski, P. Olk, L.M. Eng, C. Ziegler, B. Adolphi, E. Jaehne, The route to functional graphene oxide, ChemPhysChem, 11 (2010) 2131-2139.
[71] H. Kim, S.O. Kang, S. Park, H.S. Park, Adsorption isotherms and kinetics of cationic and anionic dyes on three-dimensional reduced graphene oxide macrostructure, Journal of Industrial and Engineering Chemistry, 21 (2015) 1191-1196.
[72] P. Montes-Navajas, N.G. Asenjo, R. Santamaría, R. Menéndez, A. Corma, H. García, Surface area measurement of graphene oxide in aqueous solutions, Langmuir, 29 (2013) 13443-13448.
[73] A.A. Jada, R. Ait, Adsorption and Removal of Organic Dye at Quartz Sand-Water Interface, Oil & Gas Science and Technology- Rev. IFP Energies nouvelles, 69 (2014) 405-413.
[74] P.R. Johnson, N. Sun, M. Elimelech, Colloid transport in physically and geochemically heterogeneous porous media_ Modeling, measurements, and parameter identification.pdf, Environmental Science and Technology, 30 (1996) 3284-3293.
[75] Y.G. Mishael, G. Rytwo, S. Nir, M. Crespin, F. Annabi-Bergaya, H. Van Damme, Interactions of monovalent organic cations with pillared clays, Journal of Colloid and Interface Science, 209 (1999) 123-128.